DESIGN AND MODELING OF SEMI-ACTIVE SQUEEZE FILM DAMPER USING MAGNETORHEOLOGICAL FLUID

Keun-Joo Kim and Chong-Won Lee
Center for Noise and Vibration Control (NOVIC),
Department of Mechanical Engineering
KAIST, Science Town, Daejeon, 305-701, KOREA
gjkim@novic.kaist.ac.kr, cwlee@novic.kaist.ac.kr

Abstract

Squeeze Film Dampers (SFDs) have been commonly used to effectively enhance the dynamic behavior of the rotating shaft supported by rolling element bearings. However, due to the recent trends of high operating speed, high load capacity and light weight in rotating machinery, it is becoming increasingly important to change the dynamic characteristics of rotating machines in operation so that the excessive vibrations, which may occur particularly when passing through critical speeds or unstable regions, can be avoided. Semi-active type SFDs using magnetorheological fluid (MR fluid), which responds to an applied magnetic field with a change in rheological behavior, are introduced in order to find its applications to rotating machinery as an effective device attenuating excessive vibration. In this paper, a semi-active SFD using MR fluid is designed, tested and modeled by means of describing function analysis to investigate the capability of changing its dynamic properties such as damping and stiffness.

Introduction

SFDs have been frequently used to overcome stability and vibration problems that cannot be adequately resolved by conventional rolling-element or journal bearings alone. One of the key design features in a SFD configuration is the introduction of support flexibility and damping in the bearing/support structure. Hence, the dynamic characteristics of SFD play an important role in the dynamic response of a rotor system. In designing a conventional SFD, an optimized damping value obtained by the consideration of the first forward mode is used to improve the stability of the system. However, this traditional design strategy becomes obsolete since the modern rotating machinery has a strong tendency of high operating speed, high load capacity and lightweight. It results in operation of a rotor at a rotational speed beyond several critical speeds, leading to the excessive vibration problems occurring when the rotor passes through the critical speeds. As an effective vibration attenuation device, controllable SFDs working in active or semi-active way are studied recently, and related research works are still in progress, including semi-active type SFDs using controllable fluid as working fluid (Morishita *et al*., 1992; Jung, 1995; Lee, *et al*., 2000).

The apparent viscosity of controllable fluid varies in response to the applied field: MR and ER fluids (Electrorheological fluids) respond to the magnetic and electric fields, respectively (Lord Material Division, 2002). In recent years, a few research results dealing with controllable SFDs have been reported: Morishita and Mitsui (1992) presented preliminary experimental results on the performance of the ER fluid based SFD (ER-SFD) and also showed its potential capability for vibration attenuation. They showed that rotor vibration could be reduced remarkably over a wide range of rotational speed by controlling the supporting damping capacity. Moreover, the existence of an optimum supporting damping for every vibration mode was shown experimentally. Jung (1995) tried to obtain the solutions for a short and open-end SFD using a modified Reynolds equation in which ER fluid is modeled as Bingham plastic

model. Lee, *et al*. (2000) also presented the vibration control performance of a pressurized, sealed, ER-SFD supported rotor. However, in spite of these research outputs, ER-SFDs have only remained as an academic interest due to the necessity of complex auxiliary devices, such as a high voltage supply, and the shortcomings of ER fluid, e.g. its sensitivity to impurities.

This work mainly focuses on the design and modeling of the proposed MR fluid based SFD (MR-SFD). First, the analysis about the magnetic characteristics of the MR-SFD is conducted to avoid magnetic saturation. Secondly, sealing system is designed to enhance the practicability of the proposed system. The designed MR-SFD is made in the laboratory and tested to obtain its dynamic model. In order to generate the excitation occurring at the real rotor system, an Active Magnetic Bearing (AMB) system is used as the exciter. Through extensive experiments, the empirical formula of the MR-SFD's dynamic stiffness is obtained and the controllability of its dynamic behavior is investigated.

Design of MR-SFD

Magnetic Circuit Analysis

In general, the maximum force available in an MR fluid based device is limited by the magnetic saturation of main components as well as MR fluid itself, which should be avoided in the preliminary design stage. The prototype MR-SFD for laboratory tests is made of SS41 steel, due to its relatively good magnetic properties, e.g. input current to magnetic field intensity ratio. The magnetic properties of SS41 are listed in Table 1.

Table 1. B-H characteristics of SS41 steel

Properties	Value
Maximum relative permeability, μ_r	893
Remnance B_r	0.78 *Tesla*
Coercive force H_c	310 *A/m*
B_s^*	1.4 *Tesla*
H_s^*	10,180 *A/m*

* : B and H at point where saturation occurs

Referring to Table 1, the magnetic field density, B, should not exceed 1.4 *Tesla* to avoid the magnetic saturation of SS41 steel.

Table 2. Properties of MRF-122-2ED (Lord Rheonetic™, 2003)

Properties	Value/Limits
Base Fluid	Hydrocarbon
Operating Temperature	-40ºC to 130ºC
Density	2.38 *g/cc*
Weight Percent Solids	72 %
Viscosity (calculated for slope between 800 1/*sec* and 500 1/*sec* at 40ºC	0.07 (± 0.02) *Pa-sec*

The working fluid, a hydrocarbon-based MR fluid given in Table 2, exhibits relatively low viscosity when no magnetic field is applied and the low viscosity is a crucial

factor for the control bandwidth.

Figure 1 shows the cross-sectional view of the designed MR-SFD. The proposed design adopts the relatively large radial clearance (0.8 *mm*) and seal's gap width (10.0 *mm*) to ensure the wide control bandwidth of the MR-SFD.

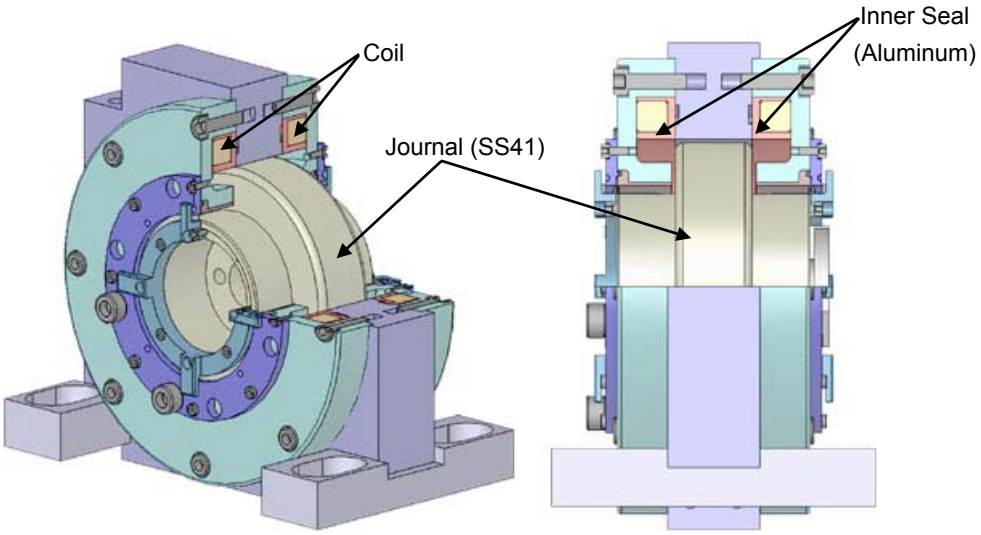

Figure 1. The proposed MR-SFD

The magnetic characteristics of the proposed MR-SFD are analyzed using the FEMM program (Meeker, 2002), for the input current of 2 *A* delivered into coils, as shown in Figure 2. Note that the maximum magnetic field density does not exceed the saturation level of 1.4 *Tesla*.

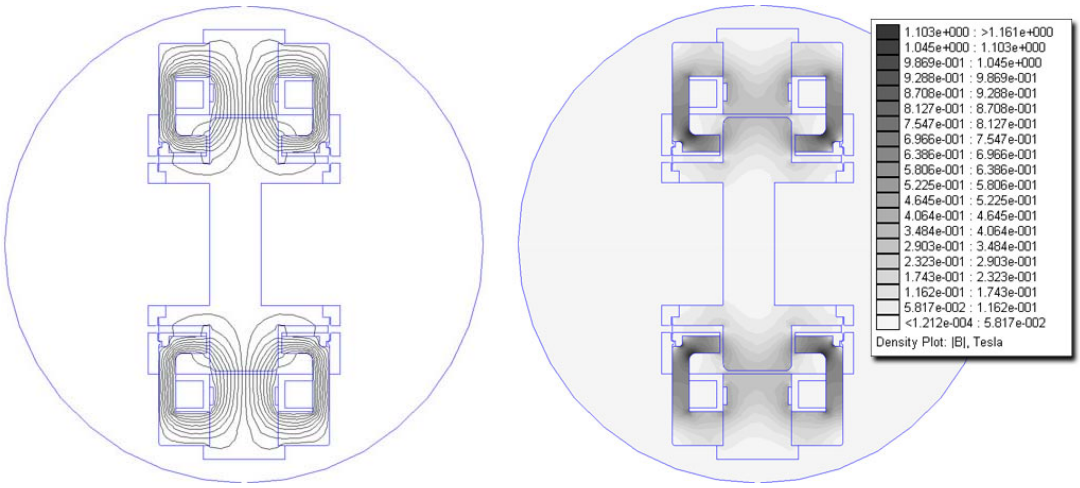

(a) Contours of magnetic flux **(b) Distribution of magnetic field density**

Figure 2. Analysis of magnetic properties of the designed MR-SFD

Sealing System Design

In the design of MR-SFD, sealing should be properly introduced, considering the abrasive property of the fluid. The required properties for sealing are:

1. fluidic tightness should be the top priority; and

2. the dynamic contribution of sealing should be negligible.

The second requirement is given to ensure wide control bandwidth of the MR-SFD. In this work, the bellows-shaped silicone seal is designed, as depicted in Figure 3.

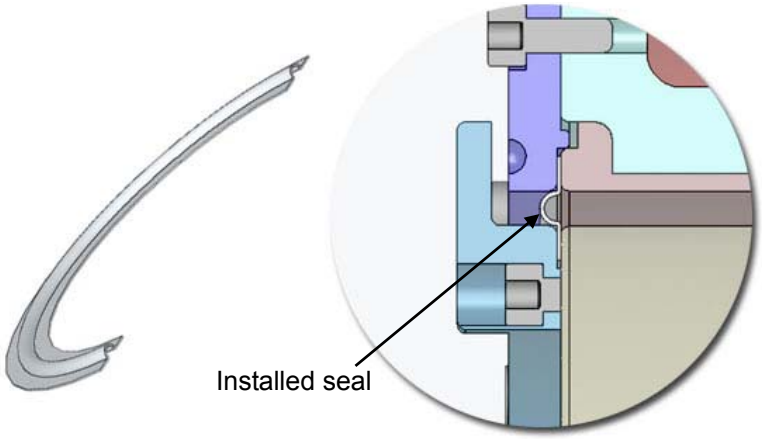

Figure 3. Bellows-shaped seal and its installation (encircled)

Equipped with the bellows-shaped seal, experiments for measurement of seal forces are conducted with no working fluid, when the peak-to-peak journal displacement of 30 μm is given. It is found that the measured force with bellows-type seal is about 1 N, about one fortieth of the force measured with an o-ring seal design. It proves that the dynamic contribution of the designed bellows-shaped sealing is sufficiently small, while its fluidic tightness is excellent.

Experimental Identification Method

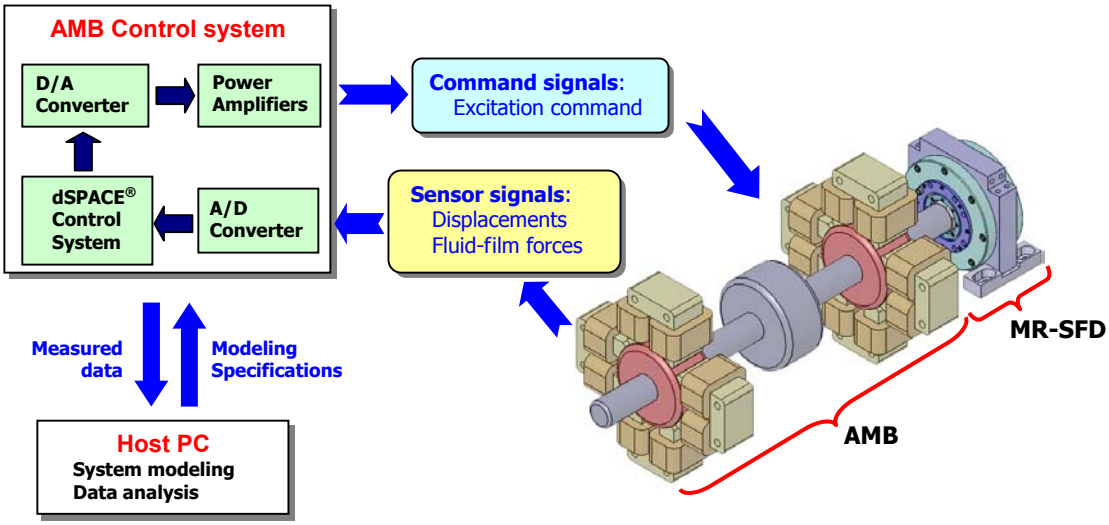

Figure 4. Scheme of experimental setup

Figure 4 shows the schematic diagram of the testing system and the input/output relationship. The shaft of AMB is supported by two radial magnetic bearings and the test MR-SFD is placed at one end of the AMB for easy assembly. Experiments are conducted in the frequency range up to 50 Hz, which is far below the first elastic mode of the AMB shaft, i.e. about 200 Hz. During the experiments, the amplitude and

frequency of the journal shaft excitation is precisely controlled by the command signals into the two radial magnetic bearing units, while the fluid film forces generated by the excitation are measured by using a tri-axis tool dynamometer installed under the MR-SFD bearing. The bearing-attached force measurement had an advantage that it can measure pure fluid effects, not requiring dynamic calibration and compensation. The journal displacements and the fluid film forces are A/D converted and saved for analysis into the host PC incorporated with a dSPACE® system. The test rig developed in the laboratory has many advantageous features including:

1. arbitrary and precise selection of the static journal operating position within the allowed clearance of AMB units,
2. contact free excitation
3. easy assembly and disassembly of test MR-SFD
4. easy adjustment of the excitation in amplitude, phase and frequency, and
5. generation of various situations which are likely to occur for real rotor-bearing systems.

Excitation of the Journal

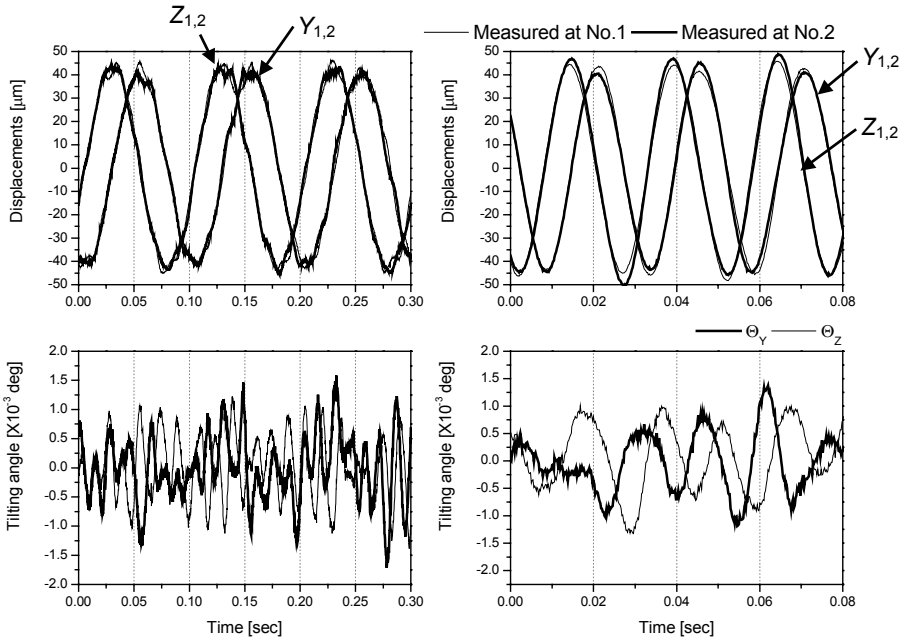

Figure 5. Excitation tests using the Filtered-X LMS algorithm

As a trade-off for easy assembly of the test MR-SFD unit to one end of the AMB system, the precise control of AMB to ensure pure translational motion of the SFD journal, subject to varying loads or disturbances, is required. In other words, the loads during test are not equally distributed over the two identical radial bearing units: one unit near the journal is subject to far severer disturbance than the other located at a distance. In this work, the Filtered X-LMS algorithm (Alexander, 1986; Clarkson, 1993; Jenkins *et al*., 1996) is adopted to ensure pure translational motion of the MR-SFD journal.

The excitation test is conducted in the frequency range up to 50 *Hz* with the frequency increment of 2 *Hz*. Figure 5 is the typical plot of the displacements, measured at the two radial magnetic bearing units, and the tilting angles of the shaft. Figures in the left column are the displacements and tilting angles of the shaft that is excited by a

harmonic command of 10 *Hz*, and those in the right are measured under a command of 40 *Hz*. The shaft displacements in the upper row of Figure 5 clearly prove the synchronized motion of the excited shaft and, therefore, the calculated tilting angles are very small. These results indicate that the excited shaft exhibit the translational motion by application of the Filtered X-LMS algorithm. Note that the tilting angles due to tracking errors at the bearing units fall within the tolerable ranges.

Signal Processing

When the test rig excites the MR-SFD journal, the generated fluid film forces in the horizontal (Z) and vertical (Y) directions are measured by the tri-axis tool dynamometer. The fluid film forces can be expressed, in terms of the displacement, velocity and acceleration of the journal under excitation, as

$$\begin{Bmatrix} F_Y \\ F_Z \end{Bmatrix} = \begin{bmatrix} K_{YY} & K_{YZ} \\ K_{ZY} & K_{ZZ} \end{bmatrix} \begin{Bmatrix} Y \\ Z \end{Bmatrix} + \begin{bmatrix} C_{YY} & C_{YZ} \\ C_{ZY} & C_{ZZ} \end{bmatrix} \begin{Bmatrix} \dot{Y} \\ \dot{Z} \end{Bmatrix} + \begin{bmatrix} M_{YY} & M_{YZ} \\ M_{ZY} & M_{ZZ} \end{bmatrix} \begin{Bmatrix} \ddot{Y} \\ \ddot{Z} \end{Bmatrix} \tag{1}$$

where F_Y and F_Z are the fluid film forces in the Y and Z directions, respectively, and K_{mn}, C_{mn}, and M_{mn} (m, n=Y, Z) represent the stiffness, damping and inertia coefficients, respectively. For the harmonic excitation of frequency ω, Eq.(1) reduces to

$$\begin{aligned} \begin{Bmatrix} F_Y(j\omega) \\ F_Z(j\omega) \end{Bmatrix} &= \begin{bmatrix} K_{YY} - \omega^2 M_{YY} + j\omega C_{YY} & K_{YZ} - \omega^2 M_{YZ} + j\omega C_{YZ} \\ K_{ZY} - \omega^2 M_{ZY} + j\omega C_{ZY} & K_{ZZ} - \omega^2 M_{ZZ} + j\omega C_{ZZ} \end{bmatrix} \begin{Bmatrix} Y(\omega) \\ Z(\omega) \end{Bmatrix} \\ &= \begin{bmatrix} D_{YY}(j\omega) & D_{YZ}(j\omega) \\ D_{ZY}(j\omega) & D_{ZZ}(j\omega) \end{bmatrix} \begin{Bmatrix} Y(\omega) \\ Z(\omega) \end{Bmatrix} \end{aligned} \tag{2}$$

The dynamic coefficients of MR-SFD can be obtained experimentally from the real and imaginary parts of the measured dynamic stiffness $D_{mn}(j\omega)$ (m, n=Y, Z).
The magnitude and phase of the measured harmonic forces and displacements of the MR-SFD journal are determined by curve fitting with harmonic signals of known frequency in the time domain (Chapra *et al*., 1998). This method has advantages that no spectral leakage occurs and no triggering/windowing is necessary, and that it is also effective even with noisy signals. For example, a measured vertical displacement signal $Y(t)$ can be approximated as a pure harmonic function $Y'(t)$ as follows:

$$Y(t) \approx Y'(t) = A_Y \sin(\omega t + \varphi) = A_Y \cos\varphi \cdot \sin\omega t + A_Y \sin\varphi \cdot \cos\omega t \tag{3}$$

In Eq.(3), the excitation frequency ω is already a known value and, therefore, the unknowns are the amplitude A_Y and the phase φ. To determine these unknown parameters, the least square error method can be applied to the measured signal as

$$\begin{bmatrix} \sin\omega t \cdot \sin\omega t & \cos\omega t \cdot \sin\omega t \\ \sin\omega t \cdot \cos\omega t & \cos\omega t \cdot \cos\omega t \end{bmatrix} \begin{Bmatrix} A_Y \cos\varphi \\ A_Y \sin\varphi \end{Bmatrix} = \begin{Bmatrix} Y(t) \cdot \sin\omega t \\ Y(t) \cdot \cos\omega t \end{Bmatrix} \tag{4}$$

In Figure 6, the curve-fit results obtained by the least square error method are plotted with the measured displacements and fluid film forces when the journal is excited in vertical direction with 25 *Hz* frequency and 0.1 *A* current input. The results shown in Figure 6 are fitting well with the measured data.

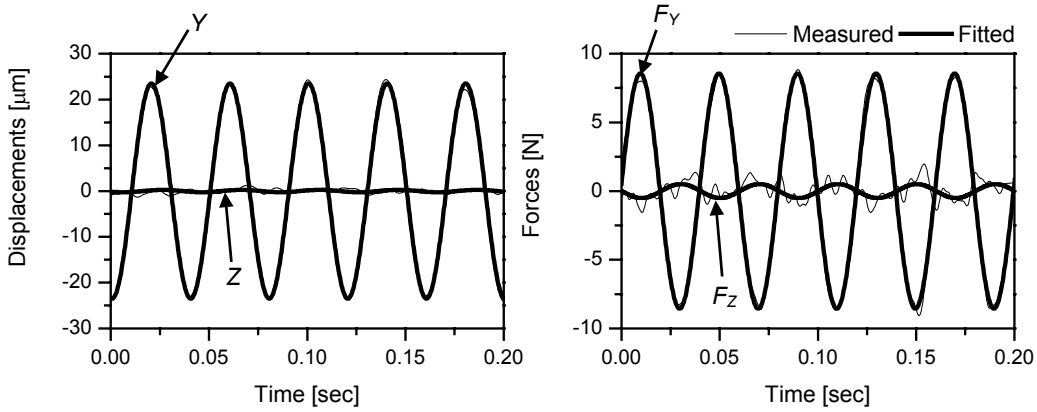

Figure 6. Measured signals vs. fitted results using the least square error method

Modeling of MR-SFD

Now, in order to get empirical expressions for dynamic stiffness of the test MR-SFD, the measured data are approximated by polynomial functions in current and frequency of excitation as

$$\begin{aligned} \mathrm{Re}\left(F_X / X\right) &= K\left(I\right) - M\left(I\right)\omega^2 \\ &= k_0 + k_1 \cdot I + k_2 \cdot I^2 - (m_0 + m_1 \cdot I)\omega^2 \end{aligned} \tag{5}$$

$$\begin{aligned} \mathrm{Im}\left(F_X / X\right) &= \Gamma\left(I\right) + C\left(I\right)\omega \\ &= \gamma_0 + \gamma_1 \cdot I + \gamma_2 \cdot I^2 + \left(c_0 + c_1 \cdot I\right)\omega \end{aligned} \tag{6}$$

Here, only direct terms of the dynamic stiffness are considered since MR-SFD is characterized by its nonrotating journal and thus the measured cross-coupled terms are also negligibly small, compared with direct terms. In Eqs.(5) and (6), the complex stiffness, $K(I)$ and $\Gamma(I)$, are modeled by polynomials of order two in current I, since these terms are related with the magnetic force and shear stress exerting on MR fluid: magnetic force is proportional to squared current while shear stress is linearly related to magnetic field density B that is proportional to current. Accordingly, the inertia $M(I)$ and the damping $C(I)$ are assumed to be linearly related to magnetic field density. Basically, the modeling scheme for the dynamic stiffness of MR-SFD, as described in Eqs.(5) and (6), by assuming the harmonic fluid film forces under harmonic excitation, is the idea of describing function analysis. In the describing function method, only the fundamental harmonic component in the nonlinear output corresponding to a harmonic input is analyzed and, therefore, the nonlinear element, in the presence of harmonic input, can be treated as if it were a linear element with a frequency response function. However, unlike the frequency response function, the magnitude of a describing function changes as input amplitude varies (Slotine et al., 1991; Khalil, 1996). First of all, we should focus on what kind of nonlinearities occur in the MR-SFD and find out their influence on the dynamic stiffness given in Eqs.(5) and (6).

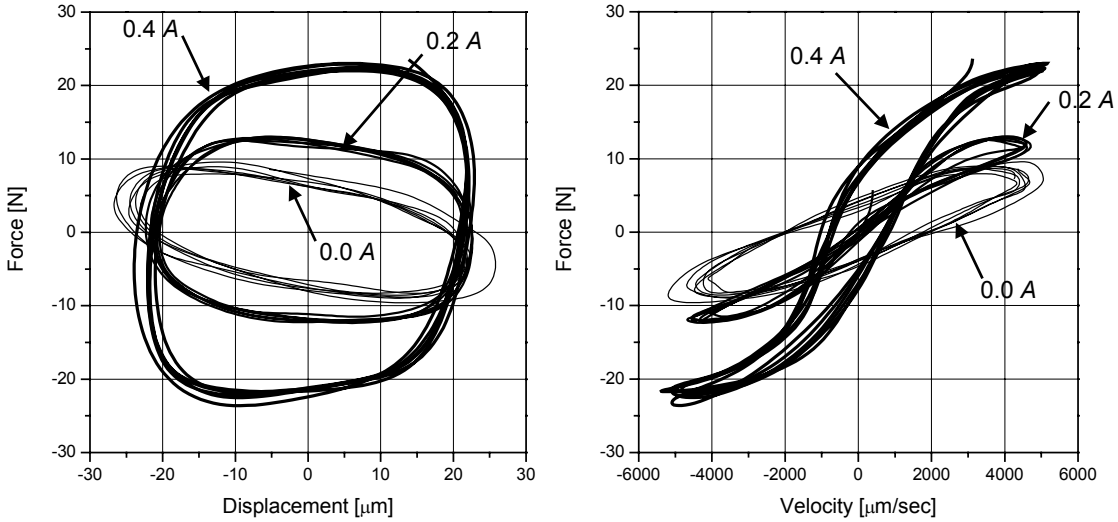

Figure 7. Nonlinear behavior of MR-SFD

Figure 7 shows the nonlinear behaviors observed in the test MR-SFD. This nonlinear behavior can be referred to as the '*shear-thinning*' effect. Liquids, in which fine particles are suspended, like MR fluids, are usually non-Newtonian. In non-Newtonian fluids, the slope of the shear stress versus shear rate curve, called the viscosity of the fluid, will not be constant as we change the shear rate.

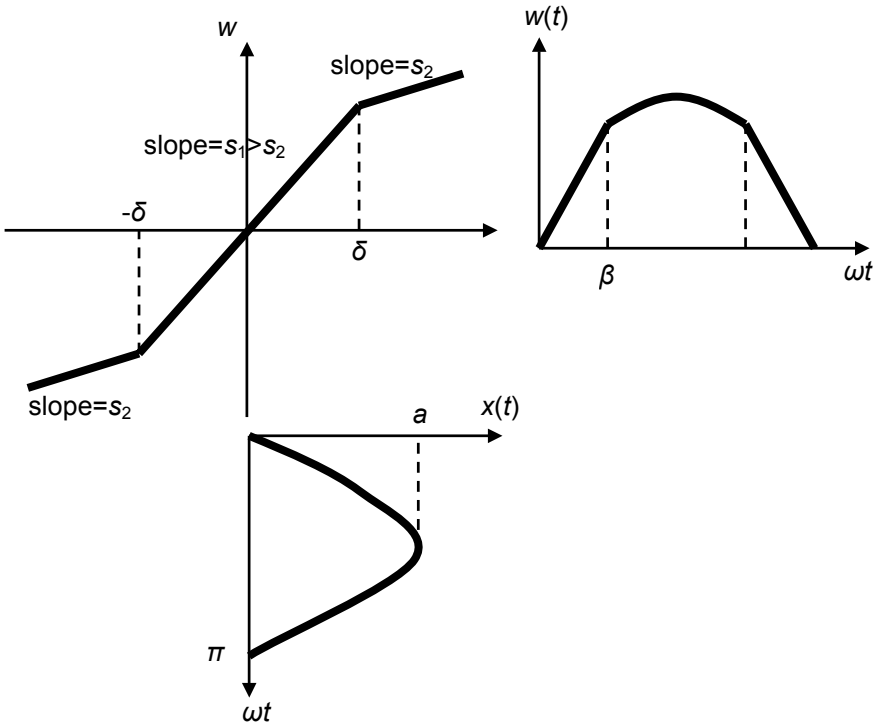

Figure 8. Piecewise-linear function

In order to analyze the shear-thinning nonlinearity by describing function, a piecewise-linear function is considered owing to its similarity with the shear-thinning phenomenon. The input/output relationships of the piecewise-linear function are described in Figure 8 and its describing function can be derived as (Khalil, 1996)

$$
\begin{aligned}
N(a) &= \frac{2}{\pi a}\int_0^{\pi} w(t)\sin(\omega t)\,d(\omega t) \\
&= \frac{4}{\pi a}\int_0^{\frac{\pi}{2}} w(t)\sin(\omega t)\,d(\omega t) \\
&= \frac{4}{\pi a}\int_0^{\beta} a s_1 \sin^2(\omega t)\,d(\omega t) + \frac{4}{\pi a}\int_{\beta}^{\frac{\pi}{2}} \left[\delta s_1 + s_2(a\sin\theta - \delta)\right]\sin(\omega t)\,d(\omega t) \\
&= \frac{2(s_1 - s_2)}{\pi}\left[\sin^{-1}\left(\frac{\delta}{a}\right) + \frac{\delta}{a}\sqrt{1-\left(\frac{\delta}{a}\right)^2}\right] + s_2
\end{aligned}
\tag{7}
$$

where, $\beta=\sin^{-1}(\delta/a)$. One can observe two crucial features in Eq.(7):

1. $N(a)=s_1$ if the input amplitude is in the linear range; and
2. $N(a)$ decreases as the input amplitude increases.

The first feature is obvious, because for small-amplitude signals the piecewise-linear behavior is not displayed at all. The second is intuitively reasonable, since piecewise-linearity amounts to reduce the ratio of the output to input. These special features could be applicable to the shear-thinning effect. In order to investigate the dependency of describing function upon input amplitude, extensive experiments were carried out under various conditions. During experiments, the input current was varied as 0.0, 0.1, 0.2, 0.3, and 0.4 *A*, and the frequency range was up to 50 *Hz*. Three different peak-to-peak input amplitudes of 40, 80, and 120 *μm* were attempted to find the dependency. Figure 9 shows the measured dynamic stiffnesses for three different input amplitudes.

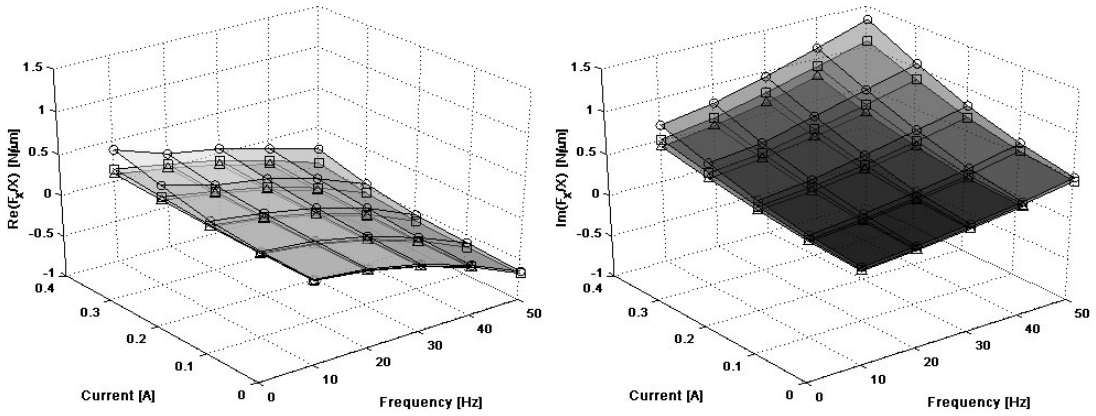

Figure 9. Dynamic stiffnesses' dependency on input amplitude
(○: 40 μm_{pp}, □: 80 μm_{pp}, △: 120 μm_{pp})

One can see that the real and imaginary parts of the dynamic stiffnesses are decreasing as the input amplitude increases and, moreover, this behavior becomes clear with high input current value. This finding can be explained by observing the data plotted in Figure 7; the shear-thinning effect becomes significant as the input current increases. Considering the input amplitude dependency on the dynamic stiffness, the empirical models, Eqs.(5) and (6), can be rewritten as

$$\begin{aligned}\mathrm{Re}\left(F_X / X\right) &= K\left(I\right) - M\left(I\right)\omega^2 \\ &= k_0 + \frac{k_2'}{X}\cdot I^2 - \left(m_0 + m_1 \cdot I\right)\omega^2 \\ &= 0.056 + \frac{39.576}{X}\cdot I^2 - \left(7.2\times10^{-3} - 3.1\times10^{-6}\cdot I\right)\omega^2\end{aligned} \tag{8}$$

$$\begin{aligned}\mathrm{Im}\left(F_X / X\right) &= \Gamma\left(I\right) + C\left(I\right)\omega \\ &= \gamma_0 + \frac{\gamma_2'}{X}\cdot I^2 + \left(c_0 + \frac{c_1'}{X}\cdot I\right)\omega \\ &= 0.075 + \frac{69.1}{X}\cdot I^2 + \left(1.26\times10^{-3} + \frac{0.072}{X}\cdot I\right)\omega\end{aligned} \tag{9}$$

Here, the input amplitude dependency is only included in each of the current-related coefficients. Besides, the first-order terms of current in the complex stiffness were removed, due to their insignificant contributions compared with the rest of terms. Using the well approximated models, Eqs.(8) and (9), the real and imaginary parts of the dynamic stiffness are plotted again in Figure 10.

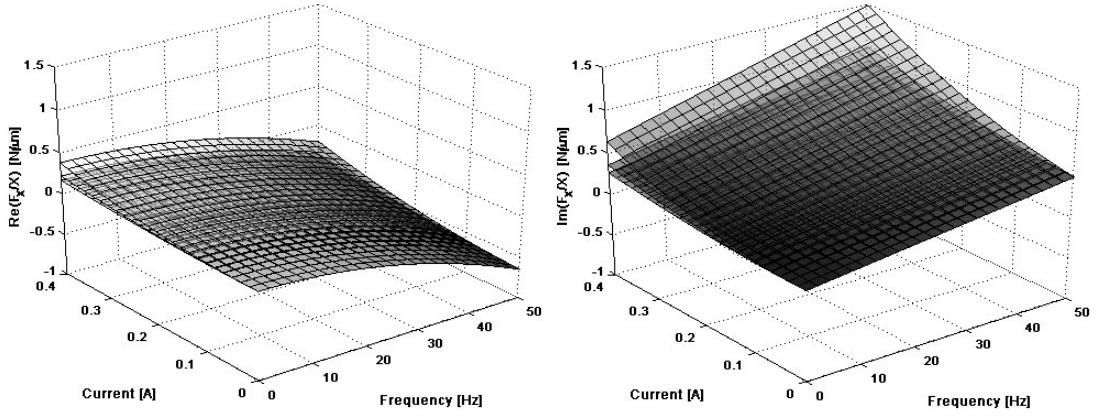

Figure 10. Estimated dynamic stiffness of the MR-SFD under varying input amplitude

Conclusions

In order to develop a controllable semi-active SFD, an MR fluid based SFD is proposed, designed and experimentally modeled. Avoiding magnetic saturation, magnetic circuit analysis is carried out and bellows-shaped silicone sealing is proposed to meet the system's practicality. Extensive experiments are conducted with the test rig utilizing an AMB system as the exciter and the measured data are analyzed, in order to model the dynamic stiffness of the designed MR-SFD. Based on the describing function concept, the dynamic characteristics are modeled as polynomial functions of frequency and input current. Moreover, the dependency of dynamic stiffness upon the input amplitude, which originates from the shear-thinning phenomenon, is investigated.

References

Alenxander, S.T. (1986), *Adaptive Signal Processing Theory and Applications*, Springer-Verlag, New York, NY.

Chapra, S.C. and R.P. Canale (1998), *Numerical Methods for Engineers* (*3rd Edition*), McGraw-Hill International Editions, Singapore.

Clarkson, P.M. (1993), *Optimal and Adaptive Signal Processing*, CRC Press, Boca Raton, FL.

Jenkins, W.K., *et al*. (1996), *Adaptive Concepts in Adaptive Signal Processing*, Kluwer Academic Publishers, Boston, MA.

Jung, S.Y. (1995), "Analysis of Short Squeeze Film Dampers Operating with Electro-Rheological Fluids," *Journal of KSTLE*, **11**, 5-11.

Khalil, H.K. (1996), *Nonlinear Systems* (*2nd Edition*), Prentice Hall, Upper Saddle River, NJ.

Lee, N.S., D.H. Choi, K.Y. Seok, Y.B. Lee, and C.H. Kim (2000), "Vibration Control of a Flexible Rotor with a Slotted-Ring Sealed Electro-Rheological Squeeze Film Damper," *IMECH 7th International Conference*, 499-506.

Lord Material Division (2002), "What is the Difference between MR and ER Fluid?," *Presentation*, May 2002.

Lord Rheonetic™ (2003), *Hydrocarbon-Based MR Fluid MRF-122-2ED Product Bulletin*, Lord.

Meeker, D. (2002), *Finite Element Method Magnetics User's Manual*, http://femm.berlios.de.

Morishita, S. and J. Mitsui (1992), "Controllable Squeeze Film Damper (An Application of Electro-Rheological Fluid," *ASME Journal of Vibration and Acoustics*, **114**, 354-357.

Slotine, J.J.E. and W. Li (1991), *Applied Nonlinear Control*, Prentice Hall, Englewood Cliffs, NJ.